

# Thermodynamics and critical behavior in the Nambu-Jona-Lasinio model of QCD

P. Costa, M. C. Ruivo, and C. A. de Sousa

*Departamento de Física, Universidade de Coimbra, P-3004-516 Coimbra, Portugal*

(Dated: July 6, 2019)

## Abstract

We investigate the phase diagram of strongly interacting matter as a function of temperature and baryonic density/chemical potential, within Nambu-Jona-Lasinio type models. We perform a systematic study concerning the existence, location and properties of a critical end point/tricritical point, both in SU(2) and SU(3) versions of the model. We verify that, for  $m_u = m_d = 0$  and up to a critical strange quark mass, there is a tricritical point, which becomes a critical end point in a world with realistic values of the current quark masses. The critical properties of physical observables as the baryon number susceptibility and the specific heat are analyzed in the vicinity of the critical end point, with special focus on their critical exponents. The behavior of mesons in the  $T - \mu_B(\rho_B)$  plane is analyzed in connection with possible signatures of partial and effective restoration of chiral symmetry.

PACS numbers: 11.30.Rd, 11.55.Fv, 14.40.Aq

## I. INTRODUCTION

Recently there have been encouraging progress on non-perturbative studies of the QCD thermodynamics which have stimulated a great deal of theoretical activity. Phenomenological and microscopic models have been developed along parallel and complementary lines allowing to predict a rich phase structure at finite temperature  $T$  and chemical potential  $\mu_B$  [1, 2, 3, 4]. The quark gluon plasm (QGP) is a longstanding theoretical issue since the discovery of the asymptotic freedom of QCD [3, 5]. Besides the intrinsic theoretical interest of this subject, such studies are important because they are directly applicable to the regime under current experimental investigation at the BNL Relativistic Heavy Ion Collider (RHIC). In fact, extensive experimental work has been done with heavy-ion collisions at CERN and Brookhaven to explore the  $T - \mu_B$  phase diagram and look for signatures of the QGP.

Theoretical studies have been accumulating a lot of evidence that there exists a critical end point (CEP) in the phase diagram of strongly interacting matter. Since Fodor and Katz, who presented a phase diagram with the CEP within lattice calculations [6], a remarkable progress in this area has been made. It is an open question, whether a critical end point exist on the  $T - \mu_B$  plane and, particularly, how to predict its location. When only thermal effects are concerned, universal arguments [7, 8] and lattice simulations [9] indicate that the order of the phase transition depends on the masses and flavors of quarks.

Considering also non-vanishing chemical potentials, a variety of models (see e.g. [10, 11]) predict a second order phase transition point in the phase diagram. This suggests that the phase diagram exhibits a CEP. At this point the phase transition is of second order and long wavelength fluctuations appear, leading to characteristic experimental consequences that can be detected by enhanced critical fluctuations in heavy-ion collisions [12, 13]. So, the location of the CEP has become an important topic in effective model studies and lattice calculations. In fact, the phase diagram and QCD thermodynamics in general are becoming more transparent due to the combination of research in several areas: perturbative QCD, effective models and lattice calculations.

The possible existence of such a point has recently been emphasized and its universal critical properties have been discussed by several authors in the context of QCD inspired models [10, 11, 14, 15]. This point of the phase diagram is the special focus of the present

article.

In a previous work [15], we studied the phase diagram focusing our attention on the CEP and the physics near it, through the behavior of the baryon number susceptibility and the specific heat; the study was performed in the framework of the SU(3) NJL model. Here, besides extending the investigation to other observables, we make a comparative study of the phase diagram in the SU(2) and SU(3) NJL models. Since more information can be taken within the simpler version of the NJL model, this systematic study is expected to provide a better understanding of the interesting physics around the CEP/TPC.

So, Nambu-Jona-Lasinio (NJL) type models are used and the main goal is to locate the critical end point and confront the results with universality arguments. Based on the fact that the CEP is a genuine thermodynamic singularity, being considered a second order critical point, the order parameter and related observables like susceptibilities can provide relevant signatures for phase transitions. We notice that susceptibilities in general are related to fluctuations through the fluctuation dissipation theorem, allowing to observe signals of phase transitions in heavy-ion reactions [16]. The specific heat  $C$ , which is related to the event-by-event temperature fluctuation [17], and mean transverse momentum fluctuations [18] in heavy-ion reactions, is also a quantity of interest in our calculation. These fluctuations should show a divergent behavior near the CEP. After equilibration the dense matter created in relativistic heavy-ion collision will expand along lines of constant entropy per baryon.

We remark that most of the work done in this area has been performed with non strange quarks only and, when strange quarks are taking into account, without mixing between the flavors  $u$ ,  $d$  and  $s$  [19]. Our SU(3) version of the NJL model includes a term that incorporates the axial anomaly of QCD, and is responsible for the mechanism of flavor mixing. We relate the discontinuity of the order parameter to other discontinuities of physical quantities such as, for instance, the entropy. We are particularly interested to confront our calculation, in what concerns to the notion of a second order phase transition due to different from zero current quark masses, with those of any classical mean field theory. From lattice calculations it is well known that the strange quark mass plays a decisive role in the location of the CEP.

On the other hand, information on the nature of excitations and the strength of their interaction in the QGP would be crucial in the experimental search. Also in this context it is relevant to confront first-principle based approaches with the results of phenomenological models like the NJL model.

We organize the work in four main steps. First, after the presentation of the model formalism (Sec. II), we discuss the behavior of the equations of state and analyze the chiral phase transition (Sec. III). The well known universality hypothesis of phase transitions will be considered. Second, we study the behavior of relevant physical quantities in the  $T - \mu_B$  plane (Sec. IV). Third, we will analyze the phase diagrams in the  $T - \mu_B$  plane looking for the location of the critical end point and the behavior of observables like susceptibilities (Sec. V). Finally, we discuss signs of *partial* and *effective* restoration of chiral symmetry (Sec. VI), looking for the convergence of chiral partners. We conclude in Sec. VII with a brief summary of our results.

## II. FORMULATION OF THE MODEL

The Lagrangian of the SU(3) NJL model [20, 21, 22] is given by

$$\begin{aligned} \mathcal{L} = & \bar{q}(i\partial \cdot \gamma - \hat{m})q + \frac{g_S}{2} \sum_{a=0}^8 \left[ (\bar{q}\lambda^a q)^2 + (\bar{q}(i\gamma_5)\lambda^a q)^2 \right] \\ & + g_D \left[ \det[\bar{q}(1 + \gamma_5)q] + \det[\bar{q}(1 - \gamma_5)q] \right]. \end{aligned} \quad (1)$$

The column vector  $q = (u, d, s)$  represents the quark field with three flavors,  $N_f = 3$ , and three colors,  $N_c = 3$ .  $\lambda^a$  are the Gell-Mann matrices,  $a = 0, 1, \dots, 8$ ,  $\lambda^0 = \sqrt{\frac{2}{3}}\mathbf{I}$ .

The Lagrangian (1) is invariant under chiral  $SU_L(3) \otimes SU_R(3)$  transformations if we put  $m_i = 0$ , where  $m_i$  are the current quark masses ( $\hat{m} = \text{diag}(m_u, m_d, m_s)$ ). The last term in (1) breaks the  $U_A(1)$  symmetry. This term is a reflection of the axial anomaly in QCD.

The model Lagrangian (1) can be put in a form suitable for the bosonization procedure after an adequate treatment of the last term, allowing to obtain a four quark interaction from the six quark interaction. Then the following effective quark Lagrangian is obtained:

$$\mathcal{L}_{eff} = \bar{q}(i\gamma^\mu \partial_\mu - \hat{m})q + S_{ab}[(\bar{q}\lambda^a q)(\bar{q}\lambda^b q)] + P_{ab}[(\bar{q}i\gamma_5\lambda^a q)(\bar{q}i\gamma_5\lambda^b q)], \quad (2)$$

where the projectors  $S_{ab}, P_{ab}$  are given by:

$$S_{ab} = g_S\delta_{ab} + g_D D_{abc} \langle \bar{q}\lambda^c q \rangle, \quad (3)$$

$$P_{ab} = g_S\delta_{ab} - g_D D_{abc} \langle \bar{q}\lambda^c q \rangle. \quad (4)$$

The constants  $D_{abc}$  coincide with the SU(3) structure constants  $d_{abc}$  for  $a, b, c = (1, 2, \dots, 8)$  and  $D_{0ab} = -\frac{1}{\sqrt{6}}\delta_{ab}$ ,  $D_{000} = \sqrt{\frac{2}{3}}$ . The hadronization procedure can be done by the integration over the quark fields in the functional integral with (2). The natural degrees of freedom

of low-energy QCD in the mesonic sector are achieved which gives the following effective action:

$$W_{eff}[\varphi, \sigma] = -\frac{1}{2} (\sigma^a S_{ab}^{-1} \sigma^b) - \frac{1}{2} (\varphi^a P_{ab}^{-1} \varphi^b) - i\text{Tr} \ln \left[ i\gamma^\mu \partial_\mu - \hat{m} + \sigma_a \lambda^a + (i\gamma_5)(\varphi_a \lambda^a) \right]. \quad (5)$$

The notation  $\text{Tr}$  stands for the trace operation over discrete indices ( $N_f$  and  $N_c$ ) and integration over momentum. The fields  $\sigma^a$  and  $\varphi^a$  are scalar and pseudoscalar meson nonets, respectively.

The first variation of the action (5) leads to the gap equations,

$$M_i = m_i - 2g_s \langle \bar{q}_i q_i \rangle - 2g_D \langle \bar{q}_j q_j \rangle \langle \bar{q}_k q_k \rangle, \quad (6)$$

with  $i, j, k = u, d, s$  cyclic.  $M_i$  are the constituent quark masses and the quark condensates are given by:  $\langle \bar{q}_i q_i \rangle = -i\text{Tr}[S_i(p)]$ ,  $S_i(p)$  being the quark Green function.

The baryonic thermodynamic potential of the grand canonical ensemble,  $\Omega(T, V, \mu_i)$ , is also obtained directly from the effective action (5). So we take the temperature  $T$ , the volume  $V$  and the chemical potential of the  $i$ -quark ( $\mu_i$ ) as the full independent state variables.

The relevant equations of state for the entropy  $S$ , the pressure  $p$  and the particle number  $N_i$ , as well as the internal energy  $E$ , follow from well known expressions like the Gibbs-Duhem relation

$$\Omega(T, V, \mu_i) = E - TS - \sum_{i=u,d,s} \mu_i N_i. \quad (7)$$

The following expressions are obtained:

$$E = -\frac{N_c V}{\pi^2} \sum_{i=u,d,s} \left\{ \int p^2 dp \frac{p^2 + m_i M_i}{E_i} (1 - n_i - \bar{n}_i) \right\} - g_S \sum_{i=u,d,s} (\langle \bar{q}_i q_i \rangle)^2 - 2g_D \langle \bar{u}u \rangle \langle \bar{d}d \rangle \langle \bar{s}s \rangle, \quad (8)$$

$$S = -\frac{N_c V}{\pi^2} \sum_{i=u,d,s} \int p^2 dp \left\{ [n_i \ln n_i + (1 - n_i) \ln(1 - n_i)] + [n_i \rightarrow 1 - \bar{n}_i] \right\}, \quad (9)$$

$$N_i = \frac{N_c V}{\pi^2} \int p^2 dp (n_i - \bar{n}_i). \quad (10)$$

$V$  is the volume of system and the quark density is determined by the relation  $\rho_i = N_i/V$ .

In the previous equations  $n_i$  and  $\bar{n}_i$  are the quark and antiquark occupation numbers

$$n_i = \frac{1}{1 + e^{\beta(E_i - \mu_i)}}, \quad \bar{n}_i = \frac{1}{1 + e^{\beta(E_i + \mu_i)}}. \quad (11)$$

We define  $\mu_B = \frac{1}{3}(\mu_u + \mu_d + \mu_s)$  and the baryonic matter density as  $\rho_B = \frac{1}{3}(\rho_u + \rho_d + \rho_s)$ . As usual, the pressure and the energy density are defined such that their values are zero in the vacuum state [23]:

$$p(\mu_i, T) = -\frac{1}{V} [\Omega(\mu_i, T) - \Omega(0, 0)], \quad (12)$$

$$\epsilon(\mu_i, T) = \frac{1}{V} [E(\mu_i, T) - E(0, 0)]. \quad (13)$$

The baryon number susceptibility is the response of the baryon number density  $\rho_B(T, \mu_i)$  to an infinitesimal variation of the quark chemical potential  $\mu_i$  [24]:

$$\chi_B = \frac{1}{3} \sum_{i=u,d,s} \left( \frac{\partial \rho_i}{\partial \mu_i} \right)_T. \quad (14)$$

Other relevant observable, in the context of possible signatures for chiral symmetry restoration in the hadron-quark transition and for transition from the hadronic matter to the QGP [24, 25, 26], is the specific heat which is defined by [15]

$$C = \frac{T}{V} \left( \frac{\partial S}{\partial T} \right)_{N_i} = \frac{T}{V} \left[ \left( \frac{\partial S}{\partial T} \right)_{\mu_i} - \frac{[(\partial N_i / \partial T)_{\mu_i}]^2}{(\partial N_i / \partial \mu_i)_T} \right], \quad (15)$$

where we have transformed the derivative  $(\partial S / \partial T)_{N_i}$  using the formula of the Jacobian. In fact, we work in the grand canonical ensemble where  $(T, V, \mu_i)$  are the set of natural independent variables (still holding  $N_i$  and  $V$  fixed).

By expanding the effective action (5) over meson fields, we get an effective meson action from which we can obtain the meson propagators. In the present work we are only concerned with  $\pi^0$  and  $\sigma$  mesons. Starting with the pseudoscalar mesons we have the effective meson action

$$W_{eff}^{(2)}[\varphi] = -\frac{1}{2} \varphi^a [P_{ab}^{-1} - \Pi_{ab}^P(P)] \varphi^b = -\frac{1}{2} \varphi^a (D_{ab}^P(P))^{-1} \varphi^b, \quad (16)$$

with  $\Pi_{ab}^P(P)$  being the polarization operator

$$\Pi_{ab}^P(P) = iN_c \int \frac{d^4 p}{(2\pi)^4} \text{tr}_D [S_i(p)(\lambda^a)_{ij}(i\gamma_5) S_j(p+P)(\lambda^b)_{ji}(i\gamma_5)], \quad (17)$$

where  $\text{tr}_D$  is the trace over Dirac matrices. The expression in square brackets in (16) is the inverse non-normalized meson propagator  $(D_{ab}^P(P))^{-1}$ .

The inverse meson propagator for  $\pi^0$  is giving by

$$D_{\pi^0}^{-1}(P) = 1 - P_{\pi^0} \Pi_{uu}^P(P), \quad (18)$$

with

$$P_{\pi^0} = g_S + g_D \langle \bar{q}_s q_s \rangle \quad (19)$$

and where the polarization operator of the  $\pi^0$  meson takes the form

$$\Pi_{uu}^P(P_0) = 4 [2I_1^u - P_0^2 I_2^{uu}(P_0)]. \quad (20)$$

The integrals  $I_1^i$  and  $I_2^{ij}(P_0)$  are given in the Appendix A.

The mass of the  $\pi^0$  meson can be determined by the condition  $D_{\pi^0}^{-1}(M_{\pi^0}, \mathbf{0}) = 0$  and the quark–meson coupling constant is evaluated as

$$g_{\pi^0 \bar{q}q}^{-2} = -\frac{1}{2M_{\pi^0}} \frac{\partial}{\partial P_0} [\Pi_{uu}^P(P_0)]_{|P_0=M_{\pi^0}}. \quad (21)$$

The procedure to describe scalar mesons is analogous. We present below the most relevant steps. Keeping now the scalar mesons only in (5), we have the effective meson action

$$W_{eff}^{(2)}[\sigma] = -\frac{1}{2} \sigma^a [S_{ab}^{-1} - \Pi_{ab}^S(P)] \sigma^b = -\frac{1}{2} \sigma^a (D_{ab}^S(P))^{-1} \sigma^b, \quad (22)$$

with  $\Pi_{ab}^S(P)$  being the polarization operator, which in the momentum space has the form of (17) with  $(i\gamma_5)$  substituted by the identity matrix.

To consider the  $\sigma$  meson we take into account the matrix structure of the propagator in (22). For the isospin symmetry considered in the present work  $\langle \bar{q}_u q_u \rangle = \langle \bar{q}_d q_d \rangle$ , and the matrices  $S_{ab}$  and  $\Pi_{ab}^S$  are reduced to

$$S_{ab} \rightarrow \begin{pmatrix} S_{33} & 0 \\ 0 & \bar{S}_{ab} \end{pmatrix} \quad \text{and} \quad \Pi_{ab}^S \rightarrow \begin{pmatrix} \Pi_{33}^S & 0 \\ 0 & \bar{\Pi}_{ab}^S \end{pmatrix}, \quad (23)$$

where the matrix elements are given in the Appendix A.

The mass of the  $\sigma$  meson can be determined by the condition  $D_{\sigma}^{-1}(M_{\sigma}, \mathbf{0}) = 0$ , where

$$D_{\sigma}^{-1} = (\mathcal{A} + \mathcal{C}) - \sqrt{(\mathcal{C} - \mathcal{A})^2 + 4\mathcal{B}^2} \quad (24)$$

with  $\mathcal{A} = S_{88} - \Delta \Pi_{00}^S(P)$ ,  $\mathcal{C} = S_{00} - \Delta \Pi_{88}^S(P)$ ,  $\mathcal{B} = -(S_{08} + \Delta \Pi_{08}^S(P))$  and  $\Delta = S_{00} S_{88} - (S_{08})^2$ .

Finally, the model is fixed by the coupling constants  $g_S$  and  $g_D$ , the cutoff in three-momentum space  $\Lambda$ , which is used to regularize the momentum space integrals and the current quark masses  $m_i$ . For numerical calculations in physical conditions we use the parameter set [22, 27, 28]:  $m_u = m_d = 5.5$  MeV,  $m_s = 140.7$  MeV,  $g_S \Lambda^2 = 3.67$ ,  $g_D \Lambda^5 =$

$-12.36$  and  $\Lambda = 602.3$  MeV, that has been determined by fixing the values  $M_\pi = 135.0$  MeV,  $M_K = 497.7$  MeV,  $f_\pi = 92.4$  MeV and  $M_{\eta' } = 960.8$  MeV. For the quark condensates we obtain:  $\langle \bar{q}_u q_u \rangle = \langle \bar{q}_d q_d \rangle = -(241.9 \text{ MeV})^3$  and  $\langle \bar{q}_s q_s \rangle = -(257.7 \text{ MeV})^3$ , and for the constituent quark masses  $M_u = M_d = 367.7$  MeV and  $M_s = 549.5$  MeV.

### III. EQUATIONS OF STATE AND PHASE TRANSITION

We will start the discussion of the phase diagram of the NJL model (1) by analyzing the behavior of the pressure/energy per particle as a function of the baryonic density, paying special attention to the Gibbs criteria. Our model of strong interacting matter can simulate either a region in the interior of a neutron star, or a hot and dense fireball created in a heavy-ion collision. In the present work we focus our attention in the last type of systems, so we impose the condition  $\mu_e = 0$  since electrons and positrons are not involved in the strong interaction. So, we naturally get the chemical equilibrium condition  $\mu_u = \mu_d = \mu_s = \mu_B$  that will be used. This choice allows for equal constituent quark masses  $M_u = M_d$  and approximates the physical conditions at RHIC. In this respect, we remind that in a relativistic heavy-ion collision of duration of  $\sim 10^{-22}$  s, thermal equilibration is possible only for processes mediated by the strong interaction rather than the full electroweak equilibrium.

Let us discuss our results for the pressure/energy per baryon at zero temperature, that are plotted in Fig. 1 as function of  $\rho_B/\rho_0$  (solid lines), where  $\rho_0 = 0.17 \text{ fm}^{-3}$  is the normal nuclear matter density. The pressure has three zeros, respectively at  $\rho_B = 0, 0.43\rho_0, 2.36\rho_0$ , that correspond to extreme of the energy per particle. For  $\rho_B < 0.2\rho_0$  the pressure and compressibility are positive, so the system can exist in a uniform gas phase, but it will not survive indefinitely, since the zero density state is energetically favored; for  $0.2\rho_0 < \rho_B < 0.43\rho_0$  the system is unstable since the compressibility is negative, in fact  $\rho_B = 0.43\rho_0$  corresponds to a maximum of the energy per particle; for  $0.43\rho_0 < \rho_B < 2.36\rho_0$ , the pressure is negative, and the third zero of the pressure,  $\rho_B = 2.36\rho_0$ , corresponds to an absolute minimum of the energy (see Fig. 1 (right panel)). The appearance of an absolute minima of the energy means the possibility for finite droplets to be in mechanical equilibrium with the vacuum at zero-pressure ( $P = 0$ ). Above  $\rho_B = 2.36\rho_0$ , that we define as  $\rho_B^{cr}$ , we have again a uniform gas phase. So, for densities  $0 < \rho_B < \rho_B^{cr}$  the equilibrium configuration is a mixed phase. This is because the Gibbs criterion of equal  $P$  and  $\mu_B$  is satisfied. So,



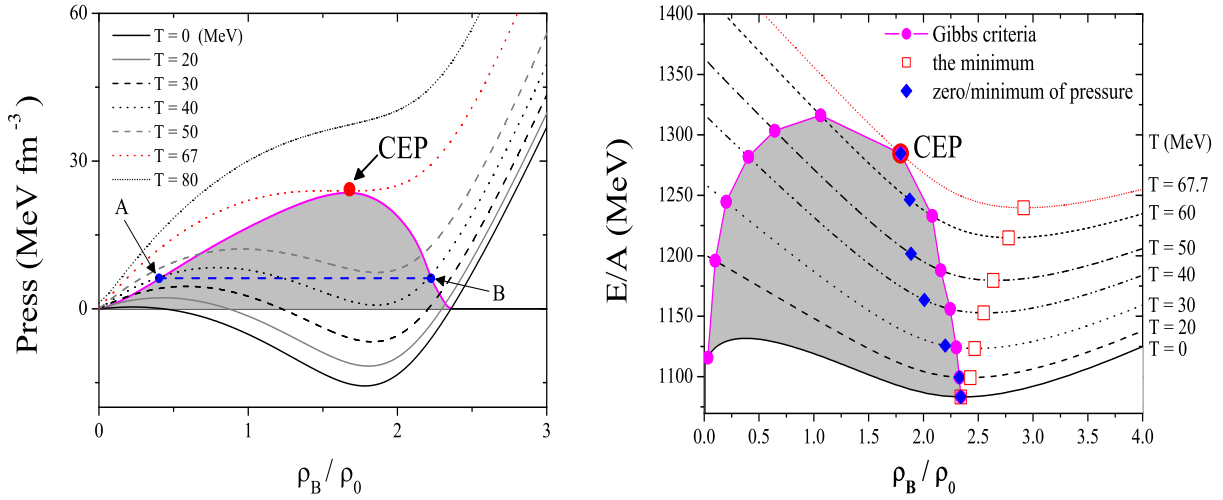


FIG. 1: Pressure (left) and energy per particle (right) as a function of the density at different temperatures. The points  $A$  and  $B$  (left panel) illustrates the Gibbs criteria. Only in the  $T = 0$  line the zero-pressure point is located at the minimum of the energy per particle.

the phase transition is a first order one: the thermodynamic potential has two degenerate minima at which two phases have equal pressure and chemical potential and can coexist. Such a situation is possible in regions where the gap equations have several solutions for the quark masses.

Summarizing the results at  $T = 0$ , the behavior described allows the following interpretation: the uniform nonzero density phase will break up into stable droplets with zero pressure and density  $\rho_B^{cr} = 2.36\rho_0$  in which chiral symmetry is partially restored, surrounded by a nontrivial vacuum with  $\rho_B = P = 0$  (see also [10, 23, 27, 29, 30]). In fact, for our choice of the parameters the critical point at  $T = 0$  satisfy to the condition  $\mu_i < M_i^{vac}$  [23, 31], where  $M_i^{vac}$  is the mass of the  $i$ -quark in the vacuum. This can be seen by comparing  $\mu_B^{cr} = 361$  MeV (see the T-axis of Fig. 2, left panel) with the quark masses  $M_u^{vac} = M_d^{vac} = 367.7$  MeV and  $M_s^{vac} = 549.5$  MeV.

As can be seen from Fig. 1, as the temperature increases, the first order transition persists up to the CEP. At the CEP the chiral transition becomes of second order. Along the line of a first order phase transition the thermodynamic potential has two degenerate minima. These minima are separated by a finite potential barrier making the potential non-convex. The height of the barrier is largest at zero temperature and finite quark chemical potential and

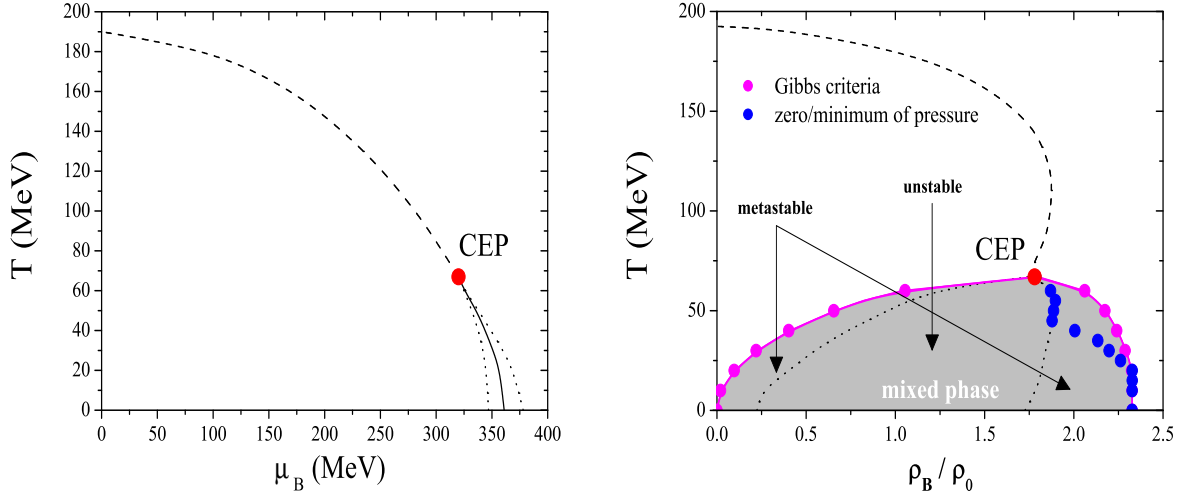


FIG. 2: Phase diagram in the SU(3) NJL model. Left (right) part corresponds to the  $T - \mu_B$  ( $T - \rho_B$ ) plane. Solid (dashed) line shows the location of the first order (crossover) transition. The dotted lines shows the location of the spinodal boundaries of the two phase transitions (shown by shading in the right plot).

decreases towards higher temperature. At the CEP the barrier disappears and the potential flattens. This pattern is characteristic of a first order phase transition: the two minima correspond, respectively, to the phases of broken and restored symmetry. The borders of the coexistence area are marked by the dotted lines in Fig. 2. The domain between the two dotted lines has metastable states which are characterized by large fluctuations. They are also solutions of the gap equations but their thermodynamic potential is higher than for the stable solutions. The left dotted curves represent the beginning of the metastable solutions of restored symmetry in the phase of broken symmetry, while the right dotted curves represent the end of the metastable solutions of broken symmetry in the restored symmetric phase. We also represent, in Fig. 2 (right panel) the region where the solutions of the gap equations are unstable.

The location of the CEP is found to be at  $T^{CEP} = 67.7$  MeV and  $\rho_B^{CEP} = 1.68\rho_0$  ( $\mu_B^{CEP} = 318.4$  MeV). For temperatures above the CEP the thermodynamic potential has only one minimum and the transition is washed out: a smooth crossover takes place.

Finally, we will focus again on the energy per baryon. In Fig. 1 (right panel), we plot the density dependence of the energy per baryon at different temperatures. We observe

that the two points, zero of pressure and minimum of the energy density, are not the same at finite temperature. In fact, as can be seen from Fig. 1 (left panel), states with zero pressure are only possible up to the maximal temperature  $T_m \sim 38$  MeV. We notice that the zero-pressure states persist up to temperatures of 70 MeV in a two-flavor NJL model where equal chemical potentials of quarks and antiquarks is assumed [29]. For  $T < T_m$  the zero-pressure states are in the metastable density region and, as soon as  $T \neq 0$ , they do not coincide with the minimum of the energy per particle.

The exposed arguments allow to clarify the difference between confined quark matter (in hadrons) and bounded quark matter (droplets of quarks). As it would be expected, the binding mechanism is weaker than the confining one (nonexistent in the NJL model). As a matter of fact, in spite of the existence of a binding energy for the droplets of quarks at  $T = 0$ , we verify that it is not possible to avoid the evaporation of the bounded quarks for arbitrarily small temperatures.

More detailed information concerning the structure of the phase diagram will be given in Sec. V.

#### IV. THERMODYNAMIC QUANTITIES IN THE $T - \mu_B$ PLANE

In this section we analyze the behavior of thermodynamic quantities such as the entropy density and the pressure in the  $T - \mu_B$  plane. We are mainly interested in the region around the CEP. We start by plotting the pressure in the left hand side of Fig. 3, which is continuous for all points of the phase diagram of the independent thermodynamic variables  $T$  and  $\mu_B$ . In the first order phase transition region ( $T < T^{CEP}$ ,  $\mu_B > \mu_B^{CEP}$ ), the entropy density (first derivative of the pressure) is discontinuous as shown in the right hand side of Fig. 3. At the crossover transition ( $T > T^{CEP}$ ,  $\mu_B < \mu_B^{CEP}$ ) thermodynamic quantities change rapidly within a narrow range of values of  $T$  and  $\mu_B$ , but the pressure and all its derivatives remain continuous as shown in Fig. 3. The discontinuity of the entropy disappears at the CEP, which location can not be determined by universality arguments. The same is not true with respect to local singular behavior of thermodynamic quantities around the CEP that will be analyzed later.

To understand the thermodynamics of matter created in relativistic heavy-ion collisions it is convenient to calculate thermodynamic quantities along lines of constant entropy per

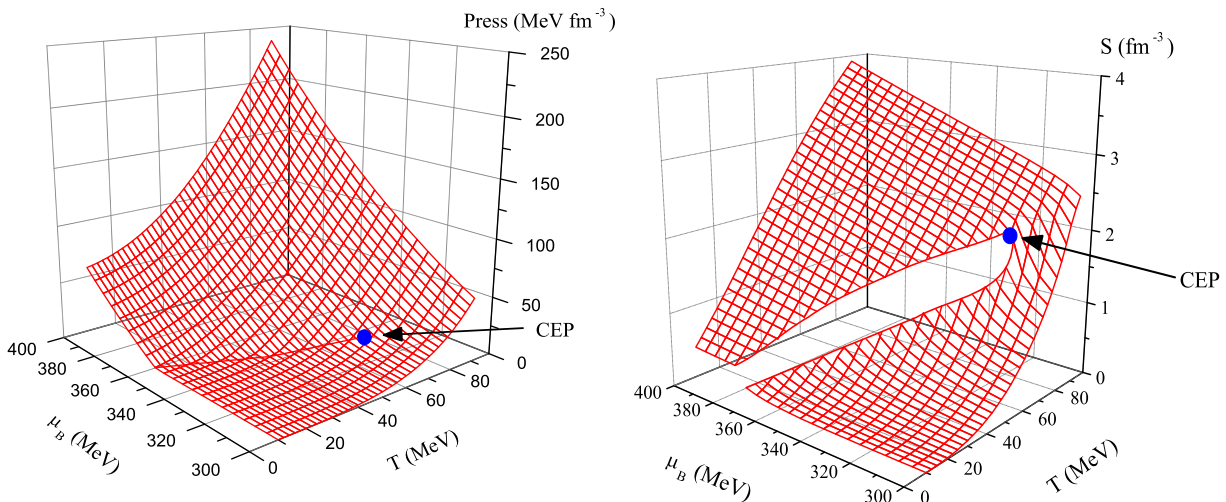


FIG. 3: Pressure (left) and entropy (right) as functions of the temperature and the baryonic chemical potential.

baryon number, the so-called isentropic lines. We notice that most of these studies have been done on lattice calculations for two-flavor QCD at finite  $\mu_B$  [32]. However, non-physical mass spectrum that corresponds to too large pion mass  $m_\pi \simeq 770$  MeV has been used. It is expected that the effects of the CEP changes only slowly as the collision energy is changed as a consequence of the attractor character of the CEP [12].

Our model calculation for the isentropic lines in the  $T - \mu_B$  plane are shown in Fig. 4. The behavior we observe is somewhat different from those claimed by other authors [32, 33, 34], where the CEP acts as an attractor of isentropic trajectories

We observe a tendency to convergence of the isentropic lines towards the CEP only in a small range of  $s/\rho_B$  around 0.7. These isentropic lines come from the region of symmetry partially restored in the direction of the crossover line. For smaller values of  $s/\rho_B$  the isentropic lines turn away from the CEP and then attain the first order transition line. For larger values of  $s/\rho_B$  the isentropic trajectories approach the CEP by the region where the chiral symmetry is still broken, and attain the first order transition line after bending toward the critical point. A similar conclusion can be found in the context of a linear sigma model and in a SU(2) NJL type model [31].

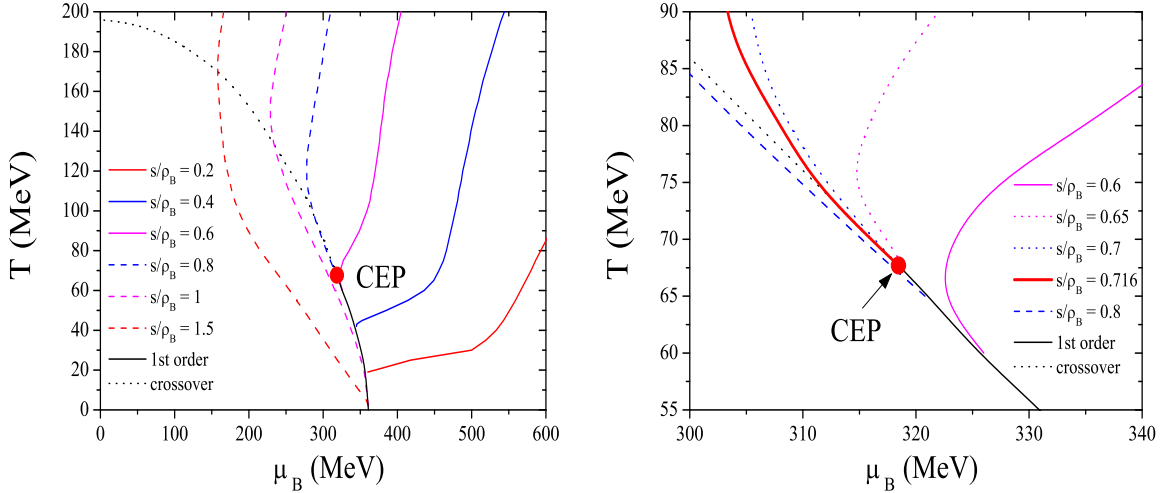


FIG. 4: Two perspectives of the entropy per baryon number in the  $T - \mu_B$  plane. The vicinity of the CEP is enlarged in the right panel. Only the contour lines of  $s/\rho_B$  constant around 0.7 are attracted by the CEP.

## V. PHASE DIAGRAMS AND SUSCEPTIBILITIES IN THE VICINITY OF THE CRITICAL END POINT

In this section we analyze with more detail the phase diagrams in different conditions in the  $T - \mu_B$  plane. Lattice QCD calculations have established the transition to a phase where quarks and gluons are deconfined at temperatures larger than  $\sim 150$  MeV and zero baryon density. Depending on the number of quark flavors  $N_f = 2$  or  $N_f = 3$ , and on the masses of the quarks, different situations can occur and the transition from hadronic matter to QGP may be of first order, second order, or a crossover transition. To confront the model results with the universality arguments, we will discuss the class of the critical points by changing the current quark masses in SU(2) and SU(3) versions of the NJL model.

### A. Characteristics of the $T - \mu_B$ phase diagram

We start by analyzing the differences between the three-flavor NJL model and its simpler version in the SU(2) sector. The phase diagrams for both models are presented in Fig. 5 as a function of  $\mu_B$  and  $T$ .

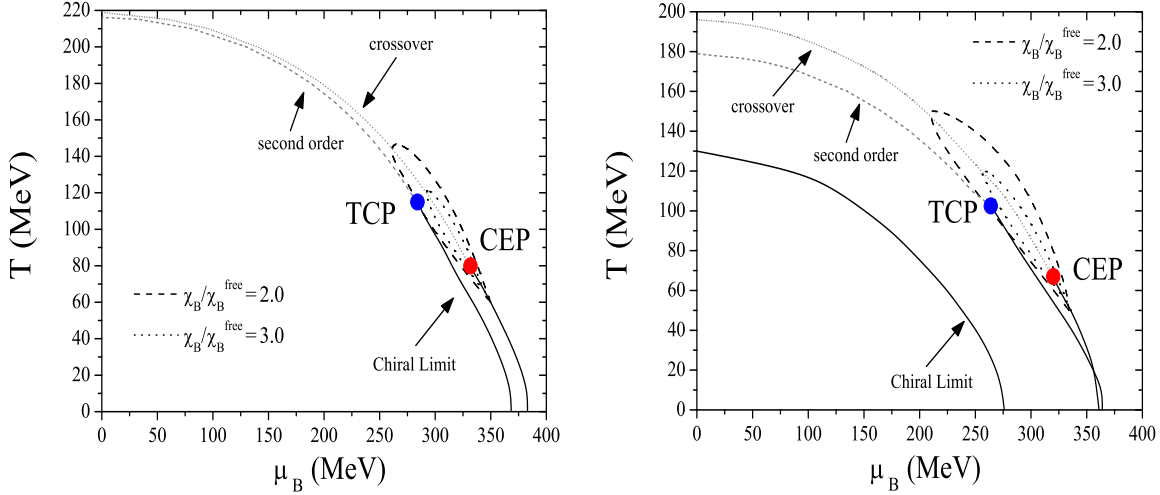


FIG. 5: Phase diagram in the SU(2) (left) and SU(3) (right) NJL models. The solid line represents the first order phase transition, the dashed line the second order phase transition and the dotted the crossover transition. The size of the critical region is also plotted for several values of  $\chi_B/\chi_B^{free}$ . The TCP in the right panel is found for  $m_u = m_d = 0$  MeV and  $m_s = 140.7$  MeV.

Concerning the SU(2) model, and using physical values of the quark masses:  $m_u = m_d = 5.5$  MeV, we find that the CEP is localized at  $T^{CEP} = 79.9$  MeV and  $\mu_B^{CEP} = 331.72$  MeV ( $\rho_B^{CEP} = 2.26\rho_0$ ). We also verified that, in the chiral limit, the transition is of second order at  $\mu_B = 0$  and, as  $\mu_B$  increases, the line of second order phase transition will end in a first order line at the TCP. The TCP is located at  $\mu_B^{TCP} = 286.1$  MeV and  $T^{TCP} = 112.1$  MeV.

For the SU(3) NJL model, also in the chiral limit ( $m_u = m_d = m_s = 0$ ), we verify that the phase diagram does not exhibit a TCP: chiral symmetry is restored via a first order transition for all baryonic chemical potentials and temperatures (see right panel of Fig. 5). This pattern of chiral symmetry restoration remains for  $m_u = m_d = 0$  and  $m_s < m_s^{crit}$  [35, 36]. In our model we found  $m_s^{crit} = 18.3$  MeV for  $m_u = m_d = 0$  [15]. When  $m_s \geq m_s^{crit}$ , at  $\mu_B = 0$ , the transition is of second order and, as  $\mu_B$  increases, the line of the second order phase transition will end in a first order line at the TCP. The TCP for  $m_s = 140.7$  MeV is the closest to the CEP [15] and is located at  $\mu_B^{TCP} = 265.9$  MeV and  $T^{TCP} = 100.5$  MeV. If we choose  $m_u = m_d \neq 0$ , instead of second order transition we have a smooth crossover which critical line will end in the first order line at the CEP. Using physical values for the

quark masses [22, 28]:  $m_u = m_d = 5.5$  MeV,  $m_s = 140.7$  MeV, this point is localized at  $T^{CEP} = 67.7$  MeV and  $\mu_B^{CEP} = 318.4$  MeV ( $\rho_B^{CEP} = 1.68\rho_0$ ).

We point out that both situations are in agreement with what is expected at  $\mu_B = 0$ : the chiral phase transition at the chiral limit is of second order for  $N_f = 2$  and first order for  $N_f \geq 3$  [37].

We also observe that the critical region is heavily stretched in the direction of the crossover transition line, in both  $N_f = 2$  and  $N_f = 3$  cases, as shown in Fig. 5. To estimate the critical region around the CEP we calculate the dimensionless ratio  $\chi_B/\chi_B^{free}$ , where  $\chi_B^{free}$  is the chiral susceptibility of a free massless quark gas. Left (right) panel of Fig. 5 shows a contour plot for two fixed ratios  $\chi_B/\chi_B^{free} = 2.0; 3.0$  in the phase diagram around the CEP.

## B. Behaviour of $\chi_B$ and $C$ in the vicinity of the critical end point and their critical exponents

The phenomenological relevance of fluctuations in the finite temperature and chemical potential around the CEP/TCP of QCD has been recognized by several authors. If the critical region of the CEP is small, it is expected that most of the fluctuations associated with the CEP will come from the mean field region around the CEP [13]. The size of the critical region around the CEP can be found by calculating the baryon number susceptibility, the specific heat and their critical behaviors.

To a better understanding of the critical behavior of the system, we also analyze in some detail what happens in the SU(2) case, sector to which there is more information in the literature [38].

As is well known, the baryon number susceptibility,  $\chi_B$ , and the specific heat,  $C$ , diverge at  $T = T^{CEP}$  [13, 15, 39]. In order to make this statement more precise, we will focus on the values of a set of indices, the so-called critical exponents, which describe the behavior near the critical point of various quantities of interest (in our case  $\epsilon$  and  $\alpha$  are the critical exponents of  $\chi_B$  and  $C$ , respectively). The motivation for this study arises from fundamental phase transition considerations, and thus transcend any particular system. These critical exponents will be determined by finding two directions, temperature-like and magnetic-field-like, in the  $T - \mu_B$  plane near the CEP, because, as pointed out in [40], the strength of the divergence is governed by the critical exponents whose values depend on the path

Quantity	critical exponents/path	SU(2) NJL	SU(3) NJL	Universality
$\chi_B$	$\epsilon / \rightarrow \bullet$	$0.66 \pm 0.01$	$0.67 \pm 0.01$	2/3
	$\epsilon' / \bullet \leftarrow$	$0.66 \pm 0.01$	$0.68 \pm 0.01$	2/3
	$\gamma_B / \rightarrow \bullet$	$0.51 \pm 0.01$	$0.49 \pm 0.02$	1/2
$C$	$\alpha / \uparrow \bullet$	$\alpha = 0.59 \pm 0.01$	$0.61 \pm 0.01$	2/3
	$\alpha / \uparrow$	$\alpha_1 = 0.45 \pm 0.01$	—	—
	$\alpha' / \downarrow \bullet$	$0.69 \pm 0.01$	$0.67 \pm 0.01$	2/3
	$\alpha / \uparrow \bullet$	$0.40 \pm 0.01$	$0.45 \pm 0.02$	1/2

TABLE I: The arrow  $\rightarrow \bullet \left( \begin{smallmatrix} \bullet \\ \uparrow \end{smallmatrix} \right)$  indicates the path in the  $\mu_B(T)$ - direction to the CEP (TCP) for  $\mu_B < \mu_B^{CEP}$  ( $T < T^{TCP}$ ).

approaching the CEP.

Considering the baryon number susceptibility, if the path chosen is asymptotically parallel to the first order transition line at the CEP, the divergence of  $\chi_B$  scales with an exponent  $\gamma_B$ . In the mean field approximation it is expected  $\gamma_B = 1$  for this path. For directions not parallel to the tangent line the divergence scales as  $\epsilon = 2/3$ . These values are responsible for the elongation of the critical region,  $\chi_B$  being enhanced in the direction parallel to the first order transition line (see Fig. 5).

To study the critical exponents for the baryon number susceptibility (Eq. 14) we will start with a path parallel to the  $\mu_B$ -axis in the  $T - \mu_B$  plane, from lower  $\mu_B$  towards the critical  $\mu_B^{CEP}$ , at fixed temperature  $T = T^{CEP}$ . Using a linear logarithmic fit

$$\ln \chi_B = -\epsilon \ln |\mu_B - \mu_B^{CEP}| + c_1, \quad (25)$$

where the term  $c_1$  is independent of  $\mu_B$ , we obtain  $\epsilon = 0.67 \pm 0.01$ , which is consistent with the mean field theory prediction  $\epsilon = 2/3$ .

We also study the baryon number susceptibility from higher  $\mu_B$  towards the critical  $\mu_B^{CEP}$ . The logarithmic fit used now is  $\ln \chi_B = -\epsilon' \ln |\mu_B - \mu_B^{CEP}| + c'_1$ . Our result shows that  $\epsilon' = 0.68 \pm 0.01$  which is very near the value of  $\epsilon$ . This means that the size of the region



we observe is approximately the same independently of the direction we choose for the path parallel to the  $\mu_B$ -axis. These critical exponents, calculated in both SU(2) and SU(3) NJL models, are presented in Table I.

For comparison purposes with the universality/mean field predictions, the calculated critical exponents at the TCP are also presented in Table I. It is found that the critical exponent for  $\chi_B$ ,  $\gamma_B$  once we are in the TCP, has the value  $\gamma_B = 0.49 \pm 0.02$ , for the SU(3) NJL model and  $\gamma_B = 0.51 \pm 0.01$ , for the SU(2) NJL model. These results are in agreement with the mean field value ( $\gamma_B = 1/2$ ), and show that the behavior of the baryon number susceptibility is similar in both SU(2) and SU(3) versions of the model.

Paying now attention to the specific heat (Eq. 15) around the CEP, we have used a path parallel to the  $T$ -axis in the  $T - \mu_B$  plane from lower/higher  $T$  towards the critical  $T^{CEP}$  at fixed  $\mu_B = \mu_B^{CEP}$ . In Fig. 6 (upper part) we plot  $C$  as a function of  $T$  close to the CEP in a logarithmic scale for both SU(2) and SU(3) calculations. In this case we use the linear logarithmic fit  $\ln C = -\alpha \ln |T - T^{CEP}| + c_2$ , where the term  $c_2$  is independent of  $T$ . Starting with the SU(2) case, we observe in the left panel that, for the region  $T < T^{CEP}$  we have a slope of data points that changes for values of  $|T - T^{CEP}|$  around 0.3 MeV. We have fitted the data for  $|T - T^{CEP}| < 0.3$  MeV and  $|T - T^{CEP}| > 0.3$  MeV separately and obtained, respectively, the critical exponent  $\alpha = 0.59 \pm 0.01$  and  $\alpha_1 = 0.45 \pm 0.01$ , which have a linear behavior for several orders of magnitude (see also Table I). As pointed out in [13], this change of the exponent can be interpreted as a crossover of different universality classes, with the CEP being affected by the TCP. It seems that in our model the effect of the hidden TCP on the CEP is relevant for the specific heat contrarily to what happens to  $\chi_B$ .

We also observe that there is no clear evidence of the change of the slope of the fitting of data points in the three-flavor NJL model (see Fig. 6, right panel of upper part, and Table I). In fact, now we only obtain a critical exponent  $\alpha = 0.61 \pm 0.01$  when the critical point is approached from below. When the critical point is approached from above the trivial exponent  $\alpha' = 0.67 \pm 0.01$  is obtained.

To explore the possible effect of the hidden TCP on the CEP, as suggested in Refs. [13, 39], we analyze the behavior of the specific heat around the TCP. As shown in Fig. 6 (lower part) and Table I, we find nontrivial critical exponents  $\alpha = 0.40 \pm 0.01$  and  $\alpha = 0.45 \pm 0.01$ , for SU(2) and SU(3) cases, respectively. This result, in spite of being close, is not in agreement

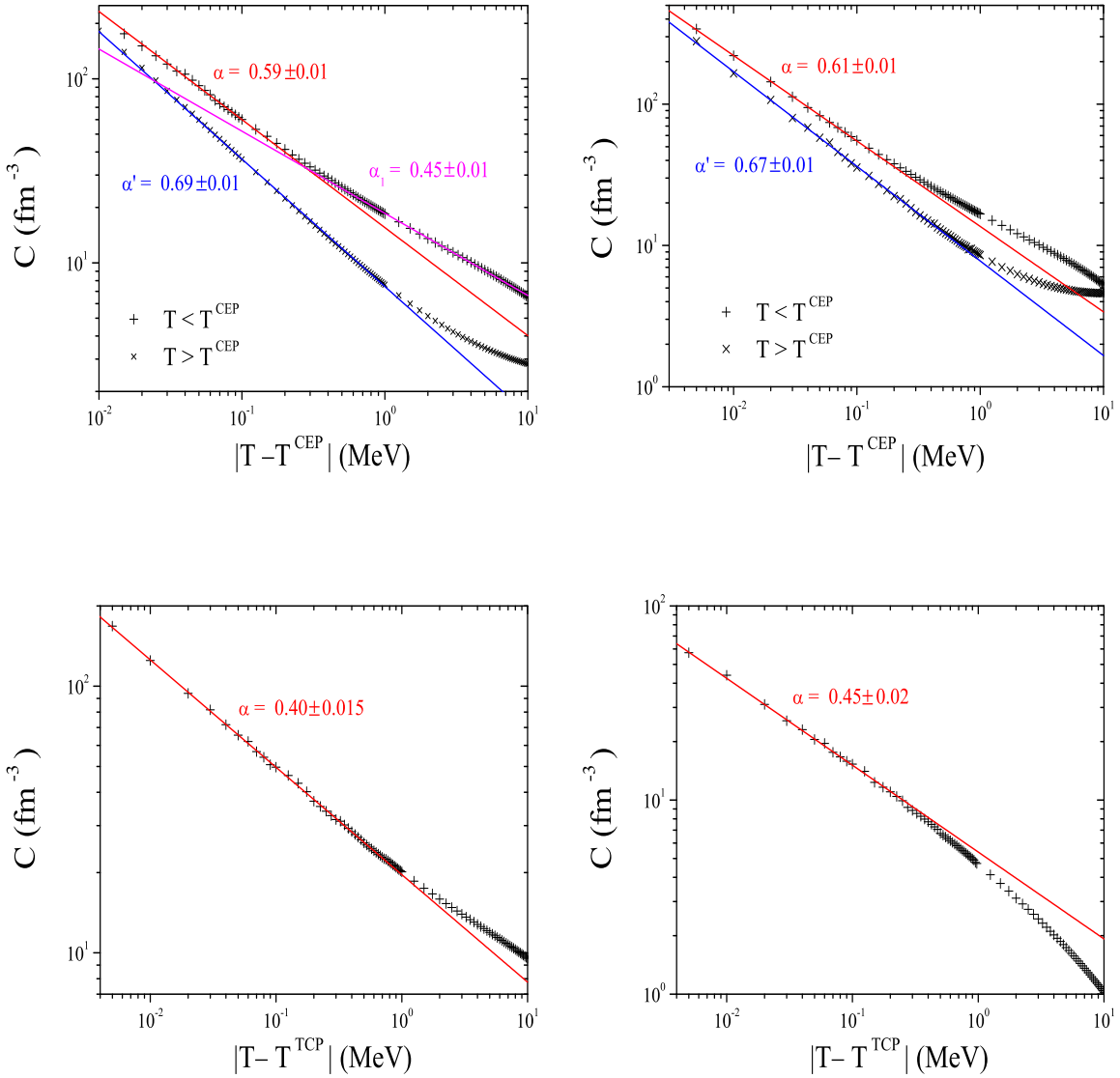


FIG. 6: Upper part: Specific heat as a function of  $|T - T^{CEP}|$  at the fixed chemical potential  $\mu_B^{CEP}$  for SU(2) (left) and SU(3) (right) NJL models. Lower part: Specific heat as a function of  $|T - T^{TCP}|$  at the fixed chemical potential  $\mu_B^{TCP}$  for SU(2) (left) and SU(3) (right) NJL models.

with the respective mean field value ( $\alpha = 1/2$ ). However, they can justify the crossing effect observed. We notice that the closest distance between the TCP and the CEP in the phase diagram occurs in the T-direction ( $(T^{TCP} - T^{CEP}) < (\mu_B^{CEP} - \mu_B^{TCP})$ ).

The inconsistency with the mean field values only occurs for the exponent  $\alpha$  as can be seen from Table I. According with what was suggested by universality arguments in [13], it

was expected that  $\chi_B$  and  $C$  should be essentially the same near the TCP and the CEP, which would imply  $\alpha = \epsilon = 2/3$  at the CEP. Nevertheless we observe that the nontrivial values of  $\alpha$  in the TCP and in the CEP are consistent within the NJL model for both, SU(2) and SU(3) versions of the model, and reflect the effect of the TCP on the CEP. We also stress that the universality arguments are so general that they give no quantitative results and, due to the lack of information from the lattice simulations, they should be confronted with model calculations. Our results seem particularly interesting because the NJL model shares with QCD some features, such as the dynamics of chiral symmetry. In particular, the physics underlying the critical singularities in the QCD diagram is associated with this fundamental property of strong interaction. So, the NJL model is an useful framework allowing for insights to the difficult task of the analysis of the QCD phase diagram at finite temperature and chemical potential.

The eventual difference between the values of the  $C$  and  $\chi_B$  critical exponents can be interesting in heavy-ion collisions experiments.

## VI. PARTIAL AND EFFECTIVE RESTORATION OF CHIRAL SYMMETRY

As we have shown in previous sections, thermodynamics provides a well established procedure, as for instance the Gibbs criterion, to determine the critical points for the phase transition in the first order region. It follows that these critical points are signaled by the discontinuity of several relevant observables (masses, quark condensates) at some critical chemical potential, a situation that does not happen in the crossover region, where these observables are continuous. At present, the criterion most commonly accepted, and that will be used here, to define the critical point in the crossover region, is to identify this point as the inflection point of the quark masses  $\partial^2 M / \partial T^2 = 0$  [23], or, equivalently, of the quark condensates [41, 42]. This criterion is numerically equivalent to the one first proposed by M. Asakawa and K. Yazaki that define the point where the constituent quark masses decrease to half of their values in the vacuum ( $M_u = M_u(0)/2$ ) [43], as the critical point. From this point on the quark masses decrease quickly.

Both in the first order and in the crossover regions it is verified that the quark masses, specially for the non strange quarks, decrease strongly at the critical point. However, at this point different observables violating chiral symmetry are still far from zero, like the

quark condensates, the pion decay constant and the difference between the masses of the chiral partners. One can say therefore that at the critical point there occurs only a *partial* restoration of chiral symmetry.

In view of what was said above we use the following criteria: we define the point in the  $T - \mu_B$  plane for the phase transition associated with *partial* restoration of chiral symmetry as the inflexion (discontinuity) point for the quark masses, and define the point for *effective* restoration of chiral symmetry as that one where the masses of chiral partners become degenerate. This is also signaled by the merging of the  $\pi^0$  and  $\sigma$  spectral functions [44]. We notice that the convergence of chiral partners only happens in the non strange sector. In fact, since the current quark mass of the strange quark is much larger than the non strange quark masses ( $m_s \gg m_u, m_d$ ), the SU(2) isospin symmetry is a much better symmetry than SU(3) flavor symmetry [27].

The behavior of the masses of the SU(2) chiral partners ( $\pi^0, \sigma$ ) in the limiting cases ( $T \neq 0, \rho_B = 0$ ) and ( $T = 0, \rho_B \neq 0$ ) are qualitatively similar and well known from the literature: they both converge at a certain value of the temperature (density). The main difference between the finite temperature and the finite density case is that, in the first one, the degeneracy of the chiral partners occurs in a range of temperatures where the mesons are no longer bound states: the  $\pi^0$  dissociates in  $q\bar{q}$  pair at the Mott temperature  $T_{M\pi^0} = 212$  MeV [22, 27], and the  $\sigma$  at the Mott temperature  $T_{M\sigma} = 160$  MeV; for the finite density case, the mesons are always bound states.

Interesting information can be obtained by calculating the masses of the  $\pi^0$  and  $\sigma$  mesons as function of  $T$  and  $\rho_B(\mu_B)$  which allows us to obtain a curve in the  $T - \rho_B(\mu_B)$  plane. This curve defines the line where the mesons became degenerate (Fig. 7). In Fig. 7 we also represent the “Mott lines” for the  $\pi^0$  and the  $\sigma$ , as well as the critical line. As it can be seen, the phase transition associated to *partial* restoration of chiral symmetry occurs above the Mott line for the pion and below the Mott line for the sigma, in most of the first order phase transition region; the opposite happens in the crossover region. Concerning the *effective* restoration of chiral symmetry, one can see, from the line of convergence of the chiral partners, that it happens after the *partial* restoration of chiral symmetry and the dissociation of the two mesons.

As we already saw, there are dramatic changes in the behavior of some thermodynamic functions such as the specific heat and the quark number susceptibilities around the CEP.

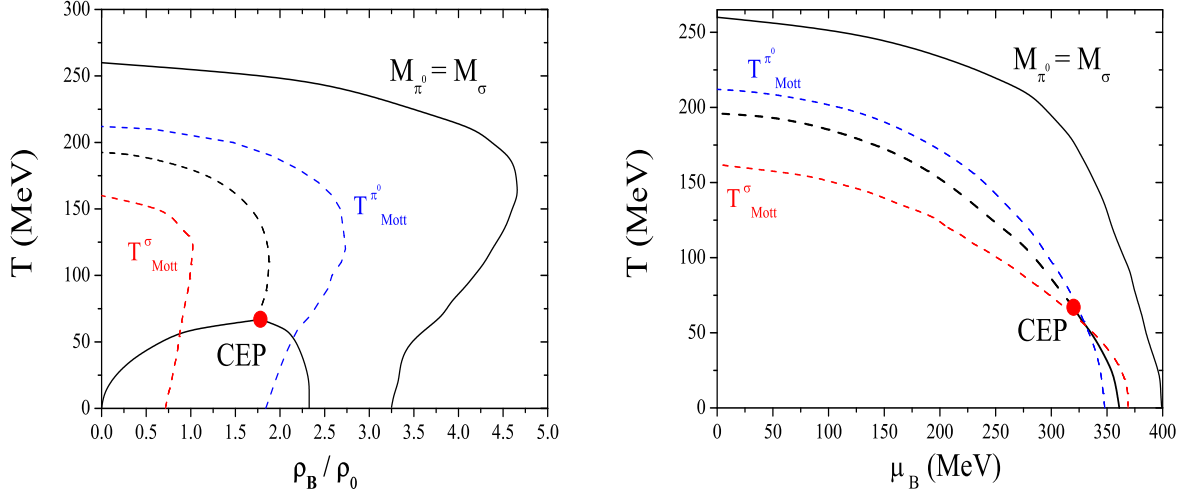


FIG. 7: The *effective* restoration of chiral symmetry, the phase transition and the Mott lines for  $\pi^0$  and  $\sigma$  mesons in the  $T - \rho_B(\mu_B)$  plane.

So, due to their role as signals for restoration of chiral symmetry it is demanding to discuss the behavior of the chiral partners ( $\pi^0$ ,  $\sigma$ ).

First we notice, in Fig. 7, that the two Mott lines cross in the first order region at a point just below the CEP. This is probably a remnant of the situation in the chiral limit where the transition is second order and the pion and sigma dissociate at the same point.

In Fig. 8 we plot the pion and sigma masses as functions of the baryonic chemical potential for three different temperatures:  $T = 40 \text{ MeV} < T^{CEP}$ ,  $T^{CEP} = 67.7 \text{ MeV}$  and  $T = 100 \text{ MeV} > T^{CEP}$ . For  $T = 40 \text{ MeV}$  and  $\mu_B \approx 350 \text{ MeV}$ , a discontinuity is visible in the evolution of the masses, signaling a first order phase transition. However, according to our criterion, the *effective* restoration of the chiral symmetry only happens at  $\mu_B \approx 380 \text{ MeV}$ . At the CEP ( $T = 67.7 \text{ MeV}$ ;  $\mu_B = 318.4 \text{ MeV}$ ), the sharp decrease (increase) of the sigma (pion) mesons masses reflect the nature of the second order phase transition. Once again the *effective* restoration of chiral symmetry only happens at  $\mu_B \approx 370 \text{ MeV}$ . When  $T = 100 \text{ MeV} > T^{CEP}$ , we have a crossover and the mesons masses have a smooth behavior. In this case, the *effective* restoration of the chiral symmetry happens at  $\mu_B \approx 355 \text{ MeV}$ .

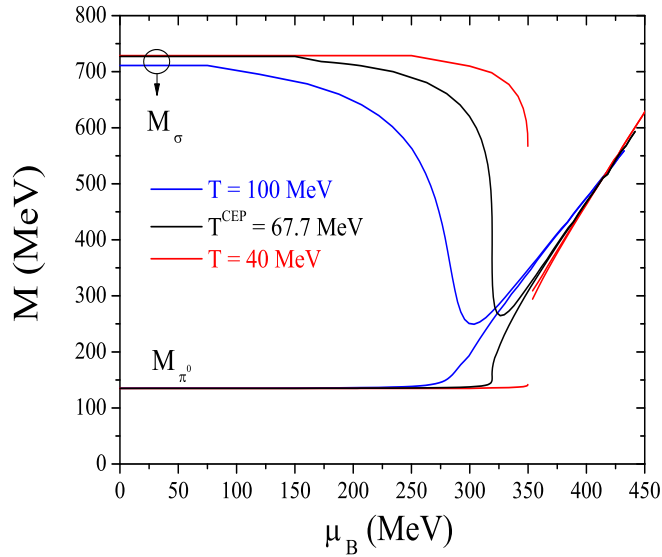


FIG. 8: Degeneracy of the chiral partners ( $\pi^0$ ,  $\sigma$ ) for different temperatures around the CEP.

## VII. CONCLUSIONS

The properties of the QCD transition at vanishing chemical potential depend on the number of quark flavors and on their masses. Critical temperature of  $T_c \approx 155$  MeV or as high as  $T_c \approx 260$  MeV have been reported in the literature. Presently, considering also non vanishing chemical potential, lattice calculations locate the CEP at  $T \approx 160$  MeV and  $\mu_B \approx 360$  MeV.

We proved that our model calculation has been able to reproduce the qualitative phase structure features, and we also obtain the location of the CEP. We have obtained, at zero baryon chemical potential in the SU(3) NJL model, values for the critical temperature around 120 – 200 MeV. The transition is first order in the chiral limit ( $m_u = m_d = m_s = 0$ ). Furthermore, when  $m_u = m_d = 0$  and  $m_s > m_s^{crit}$  ( $m_s^{crit} = 18.3$  MeV) the transition is of second order ending in a first order line at the TCP. Finally, when also  $m_u = m_d \neq 0$ , there is a crossover for all values of  $m_s$  and the location of the CEP depends strongly on the strange quark mass. Contrarily to what happens in the three-flavor NJL model, we find a TCP in the two-flavor NJL model in the chiral limit. This agrees with what is expected at  $\mu_B = 0$ : for  $m_i = 0$  the chiral restoration happens via a second order phase transition for  $N_f = 2$ , and via a first order for  $N_f \geq 3$ . For realistic values of the current quark masses the CEP

is located at  $T^{CEP} = 79.9$  MeV and  $\mu_B^{CEP} = 331.7$  MeV for  $N_f = 2$ , and at  $T^{CEP} = 67.7$  MeV and  $\mu_B^{CEP} = 318.4$  MeV for  $N_f = 3$ .

The pattern characteristic of a first order phase transition has also been analyzed through several equations of state. For example, we verified that states (droplets) in mechanical equilibrium with the vacuum state at  $P = 0$  are only possible at zero temperature. The behavior of the entropy and of isentropic lines have also been studied. We observed a tendency to convergence of the isentropic lines towards the CEP only in a small range of  $s/\rho_B$ .

We have studied the baryon number susceptibility and the specific heat which are related with event-by-event fluctuations of  $\mu_B$  or  $T$  in heavy-ion collisions. In the two and three-flavor NJL models, for  $\chi_B$ , we conclude that the obtained critical exponents around the CEP in both models are consistent with the mean field values  $\epsilon = \epsilon' = 2/3$ . For the specific heat we obtain nontrivial exponents  $1/2 < \alpha < 2/3$  around the CEP, indicating a crossover of different universality classes [13, 39]. This effect is more clearly visible for the critical exponent of the specific heat in the SU(2) version of the NJL model, where a crossover from  $\alpha$  to  $\alpha_1$  is also observed. Nevertheless we notice that the values of  $\alpha$  in the TCP and in the CEP are consistent within both versions of the NJL model. A better insight to the difficult task of the analysis of the phase diagram of QCD can be provided by an extension of the NJL model where quarks interact with the temporal gluon field represented by the Polyakov loop dynamics [4, 38, 44, 45]. Work in this direction is in progress.

Concerning the behavior of the chiral partners in the vicinity of the CEP, we verified that the two Mott lines, respectively for  $\sigma$  and  $\pi^0$  cross at a point just below the CEP. On the other hand, there is a sharp decrease (increase) of the sigma (pion) mesons masses at the CEP, what reflects the nature of the second order phase transition at this point.

### Acknowledgments

Work supported by grant SFRH/BPD/23252/2005 (P. Costa), Centro de Física Teórica, FCT under project POCI/FP/63945/2005 and under project PTDC/FP/63912/2005 (GTAE).

## APPENDIX A

In this appendix we give the integrals appearing in the meson propagators, in the vacuum and at finite temperature and density, as well as some useful expressions concerning the  $\sigma$  meson.

The integrals  $I_1^i$  and  $I_2^{ij}(P_0)$  are given by

$$I_1^i(T, \mu_i) = \frac{N_c}{4\pi^2} \int \frac{\mathbf{p}^2 d\mathbf{p}}{E_i} (1 - n_i - \bar{n}_i), \quad (\text{A1})$$

$$I_2^{ii}(P_0, T, \mu_i) = \frac{N_c}{2\pi^2} \mathcal{P} \int \frac{\mathbf{p}^2 d\mathbf{p}}{E_i} \frac{1}{4E_i^2 - P_0^2} (1 - n_i - \bar{n}_i), \quad (\text{A2})$$

where  $E_i = \sqrt{\mathbf{p}^2 + M_i^2}$  is the quark energy. To regularize the integrals we introduce the 3-dimensional cutoff parameter  $\Lambda$ . When  $P_0 > 2M_i$  it is necessary to take into account the imaginary part of the second integral. It may be found, with help of the  $i\epsilon$ -prescription  $P_0^2 \rightarrow P_0^2 - i\epsilon$ . Using

$$\lim_{\epsilon \rightarrow 0^+} \frac{1}{y - i\epsilon} = \mathcal{P} \frac{1}{y} + i\pi\delta(y) \quad (\text{A3})$$

we obtain the integral

$$\begin{aligned} I_2^{ii}(P_0, T, \mu_i) &= \frac{N_c}{2\pi^2} \mathcal{P} \int \frac{\mathbf{p}^2 d\mathbf{p}}{E_i} \frac{1}{4E_i^2 - P_0^2} (1 - n_i - \bar{n}_i) \\ &+ i \frac{N_c}{16\pi} \sqrt{1 - \frac{4M_i^2}{P_0^2}} \left[ 1 - n_i \left( \frac{P_0}{2} \right) - \bar{n}_i \left( \frac{P_0}{2} \right) \right]. \end{aligned} \quad (\text{A4})$$

Concerning the calculation of the propagator for the  $\sigma$  meson, the projector  $S_{ab}$  and the polarization operator  $\Pi_{ab}^S$  matrices, in the case  $\langle \bar{q}_u q_u \rangle = \langle \bar{q}_d q_d \rangle$ , have the nonvanishing elements

$$S_{33} = g_S - g_D \langle \bar{q}_s q_s \rangle, \quad (\text{A5})$$

$$S_{00} = g_S + \frac{2}{3} g_D (\langle \bar{q}_u q_u \rangle + \langle \bar{q}_d q_d \rangle + \langle \bar{q}_s q_s \rangle), \quad (\text{A6})$$

$$S_{88} = g_S - \frac{1}{3} g_D (2 \langle \bar{q}_u q_u \rangle + 2 \langle \bar{q}_d q_d \rangle - \langle \bar{q}_s q_s \rangle), \quad (\text{A7})$$

$$S_{08} = S_{80} = -\frac{1}{3\sqrt{2}} g_D (\langle \bar{q}_u q_u \rangle + \langle \bar{q}_d q_d \rangle - 2 \langle \bar{q}_s q_s \rangle). \quad (\text{A8})$$



Analogously, we get

$$\Pi_{00}^S(P_0) = \frac{2}{3} [\Pi_{uu}^S(P_0) + \Pi_{dd}^S(P_0) + \Pi_{ss}^S(P_0)], \quad (\text{A9})$$

$$\Pi_{88}^S(P_0) = \frac{1}{3} [\Pi_{uu}^S(P_0) + \Pi_{dd}^S(P_0) + 4\Pi_{ss}^S(P_0)], \quad (\text{A10})$$

$$\Pi_{08}^S(P_0) = \Pi_{80}^S(P_0) = \frac{\sqrt{2}}{3} [\Pi_{uu}^S(P_0) + \Pi_{dd}^S(P_0) - 2\Pi_{ss}^S(P_0)], \quad (\text{A11})$$

where

$$\Pi_{ii}^S(P_0) = 4[2I_1^i + [P_0^2 - 4M_i^2]I_2^{ii}(P_0)]. \quad (\text{A12})$$

- 
- [1] M. Alford, K. Rajagopal, and F. Wilczek, Phys. Lett. B **422**, 247 (1998); M. Alford, K. Rajagopal, and F. Wilczek, Nucl. Phys. **B537**,443 (1999).
  - [2] R. Rapp, T. Schäfer, E. V. Shuryak, and M. Velkovsky, Phys. Rev. Lett. **81**, 53 (1998).
  - [3] M. A. Halasz, A. D. Jackson, R. E. Shrock, M. A. Stephanov, and J. J. M. Verbaarschot, Phys. Rev. D **58**,096007 (1998).
  - [4] C. Ratti, M. A. Thaler, W. Weise, Phys. Rev. D **73**, 014019 (2006).
  - [5] J. Liao, and E. Shuryak, Nucl. Phys. **A775**, 224 (2006).
  - [6] Z. Fodor, S. D. Katz, J. High Energy Phys. **0204** 050 (2004).
  - [7] F. Wilczek, Int. J. Mod. Phys. **A 7**, 3911 (1992).
  - [8] K. Rajagopal and F. Wilczek, Nucl. Phys. **B399**, 395 (1993).
  - [9] A. Ukawa, Nucl. Phys. **53** (Proc. Suppl.), 106 (1997).
  - [10] M. Buballa and M. Oertel, Nucl. Phys. **A642**, 39 (1998).
  - [11] M. Buballa and M. Oertel, Phys. Lett. B **457**, 261 (1999).
  - [12] M. Stephanov, K. Rajagopal, and E. Shuryak, Phys. Rev. Lett. **81**, 4816 (1998).
  - [13] Y. Hatta and T. Ikeda, Phys. Rev. D **67**, 014028 (2003).
  - [14] T. M. Schwarz, S. P. Klevansky, and G. Papp, Phys. Rev. C **60**, 055205 (1999).
  - [15] P. Costa, C. A de Sousa, M. C. Ruivo, and Yu. L. Kalinovsky, Phys. Letts. **B 647**, 431 (2007).
  - [16] H. Appelshauser and H. Sako, for the CERES Collaboration, Nucl. Phys. **A752** 394 (2005);  
J. T. Mitchell and the PHENIX Collaboration, J. Phys. Conf. Ser. **27**, 88 (2005).
  - [17] L. Stodolsky, Phys. Rev. Lett. **75**, 1044 (1995).
  - [18] R. Korus *et al.*, Phys. Rev. C **64**, 054908 (2001).

- [19] A. Barducci *et al.*, Phys. Lett. B **231**,463 (1989); Phys. Rev. D **41**, 1610 (1990); A. Barducci *et al.*, Phys. Rev. D **49**, 426 (1994)
- [20] Y. Nambu and G. Jona-Lasinio, Phys. Rev. **122**, 345 (1961); Phys. Rev. **124**, 246 (1961).
- [21] T. Hatsuda and T. Kunihiro, Phys. Rept. **247**, 221 (1994).
- [22] P. Rehberg, S. P. Klevansky, and J. Hüfner, Phys. Rev. C **53**, 410 (1996).
- [23] M. Buballa, Phys. Rep. **407**, 205 (2005).
- [24] L. D. McLerran, Phys. Rev. D **36**, 3291 (1987).
- [25] M. Asakawa, U. Heinz, and B. Müller, Phys. Rev. Lett. **85**, 2072 (2000).
- [26] J.P. Blaizot, E. Iancu, and A. Rebhan, Phys. Lett. B **523**, 143 (2001).
- [27] P. Costa, M. C. Ruivo, C. A. de Sousa, and Y. L. Kalinovsky, Phys. Rev. C **70**, 025204 (2004).
- [28] P. Costa, M. C. Ruivo, C. A. de Sousa, and Y. L. Kalinovsky, Phys. Rev. D **70**, 116013 (2004); Phys. Rev. D **71**, 116002 (2005); P. Costa, M. C. Ruivo, and Yu. L. Kalinovsky, Phys. Lett. B **560**, 171 (2003); Phys. Lett. B **577**, 129 (2003).
- [29] I. N. Mishustin, L. M. Satarov, H. Stöcker, and W. Greiner, Phys. Rev. C **62**, 034901 (2000).
- [30] K. Rajagopal, Nucl. Phys. **A661**, 150 (1999); J. Berges and K. Rajagopal, Nucl. Phys. **B538**, 215 (1999).
- [31] O. Scavenius, A. Mocsy, I. N. Mishusti, and D. H. Rischke, Phys. Rev. C **64**, 045202 (2001).
- [32] S. Ejiri, F. Karsch, E. Laermann, and C. Schmidt, Phys. Rev. D **73**, 054506 (2006).
- [33] M. Stephanov, K. Rajagopal, and E. Shuryak, Phys. Rev. D **60**, 114028 (1999).
- [34] C. Nonaka and M. Asakawa, Phys. Rev. C **71**, 044904 (2005).
- [35] S.D.H. Hsu and M. Schwetz, Phys. Lett. B **432**, 203 (1998).
- [36] A. Barducci, R. Casalbuoni, G. Pettini, and L. Ravagli, Phys. Rev. D **72** (2005) 056002.
- [37] R.D. Pisarski and F. Wilczek, Phys. Rev. D **29**, 338 (1984).
- [38] C. Sasaki, B. Friman, and K. Redlich, Phys. Rev. D **75**, 054026 (2007); Phys. Rev. D **75**, 074013 (2007).
- [39] B.-J. Schaefer and J. Wambach, Phys. Rev. D **75**, 085015 (2007).
- [40] R. B. Griffiths and J. Wheeler, Phys. Rev. A **2**, 1047 (1970).
- [41] B. Allés, M. D’Elia, and A. Giacomo, Nucl. Phys. **B494**, 281 (1997).
- [42] M. C. Ruivo, P. Costa, C. A. de Sousa, and Yu L. Kalinovsky, J. Phys. G: Nucl. Part. Phys. **31**, S1183 (2005).
- [43] M. Asakawa and K. Yazaki, Nucl. Phys. **A504**, 668 (1989).

- [44] H. Hansen, W. M. Alberico, A. Beraudo, A. Molinari, M. Nardi, and C. Ratti, Phys. Rev. D **75**, 065004 (2007).
- [45] E. Megias, E. Ruiz Arriola, and L.L. Salcedo, Phys. Rev. D **74** (2006) 065005; Phys. Rev. D **74** (2006) 114014.